ELSEVIER

Marine Geology 127 (1995) 145–165

MARINE GEOLOGY
INTERNATIONAL JOURNAL OF MARINE GEOLOGY, GEOCHEMISTRY AND GEOPHYSICS

Late Quaternary paleoceanography of the South China Sea: surface circulation and carbonate cycles

Wang Pinxian, Wang Luejiang, Bian Yunhua, Jian Zhimi

Laboratory of Marine Geology, Tongji University, 1239 Shiping Road, 200092 Shanghai, People's Republic of China

Revision accepted 24 January 1995

Abstract

Paleoceanographic information from 34 sediment cores is summarized to investigate the glacial–interglacial variations in sea surface circulation and late Quaternary carbonate cycles in the South China Sea. Judging from the distribution pattern of deposition rates, the enormous terrigenous supply by rivers is responsible for the high rate of hemipelagic sedimentation which was even higher during glacial periods.

Paleotemperature maps based on Transfer Function temperature estimates have revealed a E–W gradient of SST for glacial summer and a S–N gradient for glacial winter, and this agrees well with the clockwise surface circulation in summer and counterclockwise in winter during glacials, as shown by a preliminary computer modelling. The high-resolution paleotemperature curves of core V36-3 from the northern slope show an abrupt cooling event which may belong to the Younger Dryas.

Carbonate percentage in sediments and preservation of foraminifers and pteropods are used to study the carbonate cycles in the marginal sea. It turns out that two mechanisms are functioning there. Being a basin with large drainage areas, vast amount of river-borne terrigenous input dilutes carbonate, and its intensification during glacial decreases the glacial $\%CaCO_3$; being a basin connected with the Pacific, the fluctuations of lysocline, CCD and ACD in the SCS are related to those in the Pacific Ocean, and dissolution is strengthened at interglacial. Thus, above the present CCD the dilution factor predominates and the "Atlantic cycles" are produced; below the present CCD the dissolution factor prevails, resulting in the "Pacific" pattern of carbonate cycles.

1. Introduction

The South China Sea (SCS) offers a special attraction for paleoceanographers because of the high sedimentation rate of its deep-marine sediments. Cores V35-5 and V35-6 taken from its southern part were among the first cores in the world ocean used for high-resolution stratigraphy documented by AMS ^{14}C datings (Andree et al., 1986; Broecker et al., 1988a), and for reconstruction of paleoventilation history in the Pacific (Berger, 1987). Recently, the SCS is intensively studied for its response to the last deglaciation (Broecker et al., 1988b; Duplessy et al., 1991; Kudrass et al., 1992; Wang et al., 1992a). As a West Pacific marginal sea with a large area above CCD, the SCS offers the opportunity to examine glacial–interglacial changes in SST (Wang and Wang, 1990), productivity (Winn et al., 1992; Thunell et al., 1992) and paleoenvironmental interactions between land and sea (Wang and Sun, 1995).

Since the 1980s, Chinese geoscientists on both sides of the Taiwan Strait have shown growing interest in paleoceanography with their emphasis laid on late Quaternary history of the SCS (for a review see Wang, in press). Tens of research papers and several volumes have been contributed to the

SSDI 0025-3227(95)00008-9

topic, most of which were published in Chinese. The present study is an attempt to pool together the data resulted from our studies and those from the English and Chinese literature, in order to find out characteristic features of the marginal sea in surface water circulation and carbonate sedimentation during the glacial cycles.

2. Stratigraphy and sedimentation

At least 34 sediment cores in the SCS have been analyzed and studied for its paleoceanography to various extends (Fig. 1; Table 1). Apart from those on the continental shelf, the cores range from 1 to 13 m in length and consist mainly of calcareous silty clay. According to oxygen-isotopic, biostratigraphic and carbonate stratigraphies, the cores have penetrated late Quaternary sequence up to oxygen isotope stage 2 to stage 8. In the present study the high-resolution chronostratigraphy based upon a stacked oxygen-isotope stratigraphy (Martinson et al., 1987) is adopted. The last appearance of pink-pigmented *Globigerinoides ruber* at about 120 kyr B.P. in the Indo-Pacific region (Thompson et al., 1979) is used as the most useful biostratigraphic marker in the SCS (P. Wang et al., 1986). Utilizing the similarity of carbonate curves between stations, carbonate stratigraphy is applied to the late Quaternary sequence in the SCS and the Okinawa Trough (Wang, 1990).

The SCS extends over an area of 3,500,000 km^2 and has an average depth of 1212 m. The shallow water part less than 200 m in depth makes up about 52% of its total area and is blanketed mostly by sandy sediments, along with mud zone characteristic of the inner shelf near the Pearl, Mekong and Red River mouths. The major topographic feature of the SCS is a deep basin of rhomboid shape with a maximum depth of 5377 m, and large reef-studded shoal areas occur within the basin to the northwest (Xisha Islands and Zhongsha Islands) and south (Nansha Islands). The central part of the basin is an abyssal plain below CCD (3500–3800 m in the SCS) covered with deep-sea clay (Fig. 2), but the sedimentation rate there reaches 2.5–7.1 cm/kyr in the Holocene, over 10 cm/kyr in the last glaciation, or one order of magnitude higher than in the open ocean (0.2–1.0 cm/kyr) (Wang et al., 1992b).

As seen from Fig. 1, most of the cores studied in the SCS have been taken from its continental slope where calcareous silty clay and clayey silt is predominant (Fig. 2). The sedimentation rate in the continental slope ranges from 0.7 to 15 cm/kyr for the Holocene and 1.3–31 cm/kyr for the last glaciation (Table 1), with the maximum values occurring in two areas: a northern area off the Pearl River mouth and a southwestern area to the northeast of the paleo-North Sunda River (Fig. 1) (Wang et al., 1992b).

When the calculated sedimentation rates at deeper water stations (more than 1900 m) are plotted against water depths, it becomes clear that the maximum rate for each depth interval declines with increase of water depth and the sedimentation rate is almost doubled in the glacial than post-glacial (Fig. 3).

3. Sea surface temperature and circulation

3.1. Previous work

Paleo-SST (sea surface temperature) estimation in the SCS started from its northern slope. Cores V36-3 and V36-8 (see Table 1; Fig. 1) were the first studied for its late Quaternary SST history with the paleo-SSTs estimated either by using optimal temperature of planktonic foraminiferal species in the modern ocean (P. Wang et al., 1986) or by applying Transfer Function technique (Samodai et al., 1986; Wang and Wang, 1989).

Later, SST fluctuations since the last 200 kyr have been studied in three sediment cores from the northern slope (V36-3, V36-5, SO49-8KL), and the discovered enhanced glacial–interglacial SST contrasts in this marginal sea have led us to a speculation on the glacial sea surface circulation in the enclosed basin (Wang and Wang, 1990). Now paleo-SST data are available at least from ten sediment cores in various parts of the SCS, and it is possible to reconstruct the glacial SST patterns and the corresponding surface circulation.

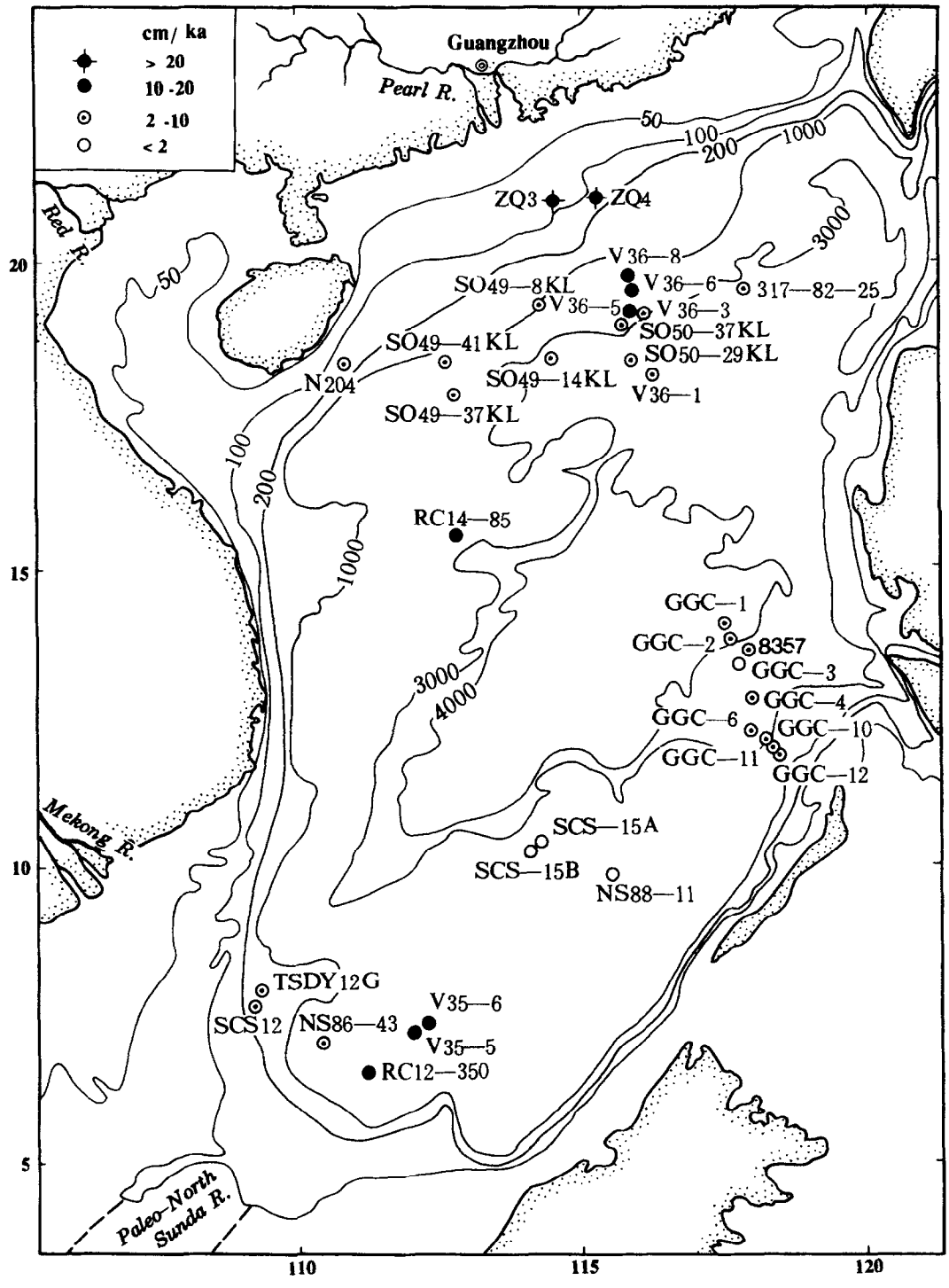

Fig. 1. Location of 34 sediment cores used in the present study with indication of the Holocene deposition rate (for details and sources see Table 1). Dashed lines denote paleo-river system.

Table 1
Sedimentation rates (cm/kyr) at 34 sites in the South China Sea during $\delta^{18}O$ stages 1 and 2

Core	Location		Water depth (m)	Core length (cm)	Total rate		$CaCO_3$%		$CaCO_3$ rate		Non-$CaCO_3$ rate		References
	°N	°E			1	2	1	2	1	2	1	2	
ZQ3	20°57′	114°30′	89	12000	77.5	2.7*							Min et al. (1992)
ZQ4	21°00′	115°25′	124	12000	42.5	27.9*							
N204	18°13′	110°56′	180	440	3.7	4.9*							Gao et al. (1992)
SCS-12	7°42′	109°18′	543	120	6.3								new data
TSDY12G	~8°	~109°	850	160	10.0								Rottman (1979)
NS88-11	9°56′	115°37′	880	433	1.0	1.3*							Li et al. (1992)
SO49-8KL	19°11′	114°12′	1040	955	3.2	8.3							Wang and Wang (1990)
V36-8	20°03′	115°43′	1304	1287	20.0								Samodai et al. (1986)
SCS-15B	10°19′	114°11′	1500	735	0.7	3.1							Wang and Chen (1990)
V36-6	19°47′	115°49′	1579	1263	10.0	8.4*	23.7	19.3*	2.4	1.6*	7.6	6.8*	Feng et al. (1988)
GGC-10	11°43′	118°31′	1605	150	3.3	7.5	46.9	40.5	1.5	3.0	1.8	4.5	Thunell et al. (1992)
NS86-43	7°02′	110°24′	1763	300	3.8	5.4							Li et al. (1992)
SCS-15A	10°25′	114°14′	1812	295	1.5	5.2	69.6	45.5	1.0	2.4	0.5	2.8	Wang et al. (1986)
RC12-350	6°33′	111°13′	1950	1129	13.3	20.7	20.9	7.1	2.8	1.5	10.5	19.2	Jian (1992)
V35-5	7°11′	112°05′	1953	1625	15.0	31.0	14.8	5.8	2.2	1.8	12.8	29.2	Broecker et al. (1988b)
SO49-37K1	17°49′	112°47′	2004	1310	4.2	4.8*							Hao et al. (1989)
V35-6	7°13′	112°09′	2030	102	13.0								Broecker et al. (1988a)
SO49-41K1	18°17′	112°41′	2120	1300	2.9	4.4*							Hao et al. (1989)
GGC-11	11°53′	118°20′	2165	145	3.8	5.8	45.4	35.7	1.7	2.1	2.1	3.7	Thunell et al. (1992)
V36-5	19°26′	115°55′	2332	1070	10.8	12.7*							Wang and Wang (1990)
RC14-85	15°25′	113°49′	2470	688	12.0								Wang et al. (1992)
GGC-12	11°56′	118°13′	2495	150	2.9	4.2	43.0	39.8	1.2	1.7	1.7	2.5	Thunell et al. (1992)
SO50-37K1	18°55′	115°46′	2695	863	10.0	16.7	26.8	14.7	2.7	2.5	7.3	14.2	Zheng and Chen (in press)
V36-3	19°01′	116°06′	2809	1215	6.8	11.0*	21.4	13.5*	1.5	1.5*	5.3	9.5*	Wang and Wang (1990)
GGC-6	12°09′	118°04′	2975	150	2.9	4.2	39.6	36.9	1.1	1.5	1.8	2.7	Thunell et al. (1992)
317-82-25	19°30′	117°53′	3205	293	4.8	4.3							Gu et al. (1991)
GGC-4	12°39′	117°56′	3530	150	2.1	5.8	21.4	27.0	0.4	1.6	1.7	4.2	Thunell et al. (1992)
SO49-14K1	18°18′	114°24′	3624	1315	4.2	13.8							Bian et al. (1992)
GGC-3	13°16′	117°48′	3725	150	1.7	3.3	6.5	18.2	0.1	0.8	1.6	2.7	Thunell et al. (1992)
SO50-29K1	18°20′	115°59′	3766	1023	7.1	16.3	8.5	9.8	0.6	1.6	6.5	14.7	Zheng and Chen (in press)
V36-1	18°04′	116°11′	3821	906	2.5	10.0*	5.3	7.4*	0.1	0.7*	2.4	9.3*	Feng et al. (1988)
8357	13°29′	118°01′	3949	383	3.3	9.6	10.6	12.5	0.3	1.2	3.0	8.4	Li (1993)
GGC-2	13°37′	117°41′	4010	125	2.5	3.3	5.4	24.8	0.1	0.8	2.4	2.5	Thunell et al. (1992)
GGC-1	14°00′	117°30′	4203	150	2.9	3.3	2.9	20.9	0.1	0.1	2.8	3.2	Thunell et al. (1992)

* Average value for stages 2–4. "1" and "2" denote $\delta^{18}O$ stages.

3.2. Materials and methods

The ten cores under discussion were taken by American, German and Chinese research vessels, and the paleo-SST estimations were performed mainly by Chinese paleoceanographers. Five of those are from the northern slope of the SCS: V36-3 (19°01′N, 116°06′E, depth 2809 m, length 1215 cm; Wang and Wang, 1989, 1990), V36-5 (19°26′N, 115°55′E, 2332 m, 1070 cm; Wang and Wang, 1990), V36-8 (20°03′N, 115°43′E, 1304 m, 1287 cm; Samodai et al., 1986), SO49-8KL (19°11′N, 114°12′E, 1040 m, 955 cm; Wang and Wang, 1990) and N204 (18°13′E, 110°56′N, 180 m, 440 cm; Gao et al., 1992); the rest 5 are from the southern part: SCS-12 (7°42′N, 109°18′N, 543

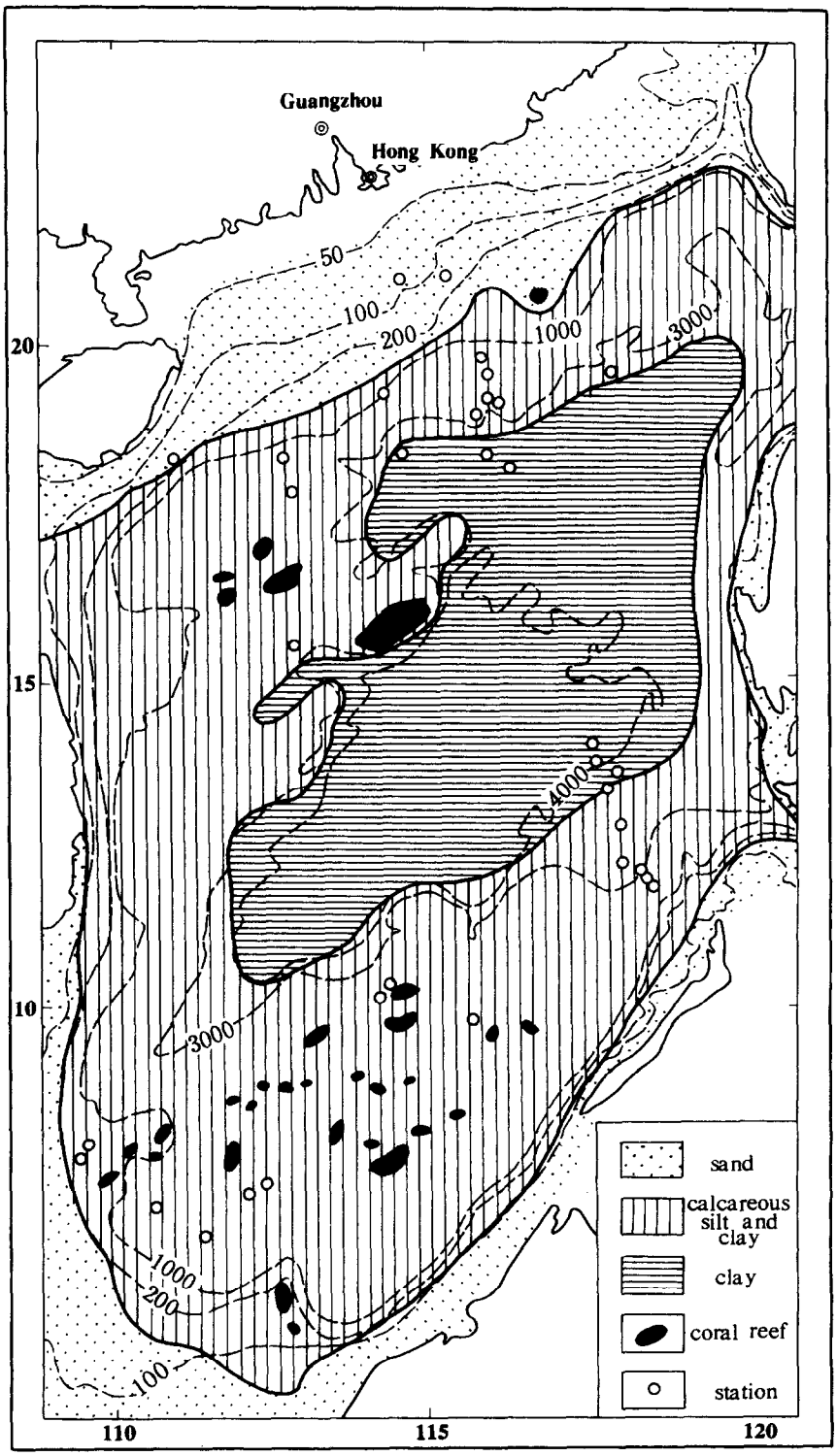

Fig. 2. Sketch map showing the distribution of bottom sediment types in the South China Sea (from P. Wang et al., 1992).

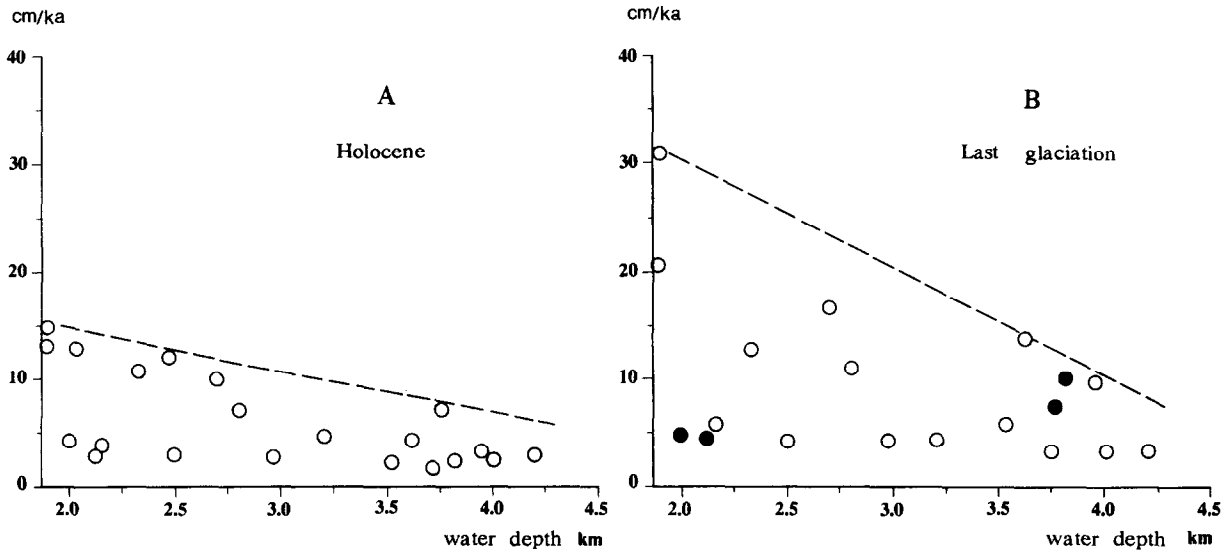

Fig. 3. Deposition rates at deeper sites (water depth >1900 m) in the South China Sea (data from Table 1). (A) Holocene; (B) last glaciation.

m, 118 cm), NS86-43 (7°02′N, 110°24′E, 1763 m, 300 cm; Li et al., 1992), RC12-350 (6°33′N, 111°13′E, 1950 m, 1129 cm; Jian, 1992), NS88-11 (9°56′N, 115°37′E, 880 m, 433 cm; Li et al., 1992) and GGC-11 (11°53′N, 118°20′E, 2165 m, 145 cm; Thunell et al., 1992) (Fig. 1).

All paleo-SST estimates are based on the downcore census data of planktonic foraminifers using the Paleoecological Transfer Function FP-12E developed by Thompson (1981) for the Western Pacific. The resulted estimates of winter and summer SST are all greater than 14° and 23°C, respectively, falling in the range in which the Transfer Function FP-12E can provide statistically accurate temperature results.

3.3. Sea surface temperature

Late Quaternary paleo-SST curves for five of the cores are given in Fig. 4. Micropaleontological analyses have shown remarkably higher percentages of temperate species such as *Neogloboquadrina pachyderma* (dextral coiling), *N. dutertrei* and *Globorotalia inflata* in the glacial section of the cores than in the Holocene (P. Wang et al., 1986) giving rise to significant downcore changes in winter SST. Thus, in the northern SCS the glacial–interglacial (G/IG) contrasts (differences between stages 2 and 5) in winter SST reach 6.8°–9.3°C, while the amplitude of summer SST fluctuations there is only 2°–3°C (Wang and Wang, 1990). These are very high values for the latitudes of the SCS which extends from the Equator to the Tropic of Cancer. Using the same transfer function, Thompson (1981) estimated the G/IG changes in tropical and subtropical region of the open Pacific as about 3°C for winter and 2°C or less for summer. Only in the temperate region between 30°N and 40°N, the G/IG SST contrast may be as mush as 5°C.

When the winter and summer SST estimates at the last glacial maximum (LGM) from the ten cores are plotted on a map, different SST patterns between winter and summer attract attention

Fig. 4. Late Quaternary paleotemperature curves at five sites in the South China Sea, showing oxygen isotope variations of *Globigerinoides sacculifer*, winter and summer SST based on planktonic foraminifers using Transfer Function FP-12E (Thompson, 1981). V36-3, SO49-8KL, V35-5 modified from Wang and Wang (1990); RC12-350 after Jian (1992); GGC-11 after Thunell et al. (1992). For location see Fig. 1 and Table 1.

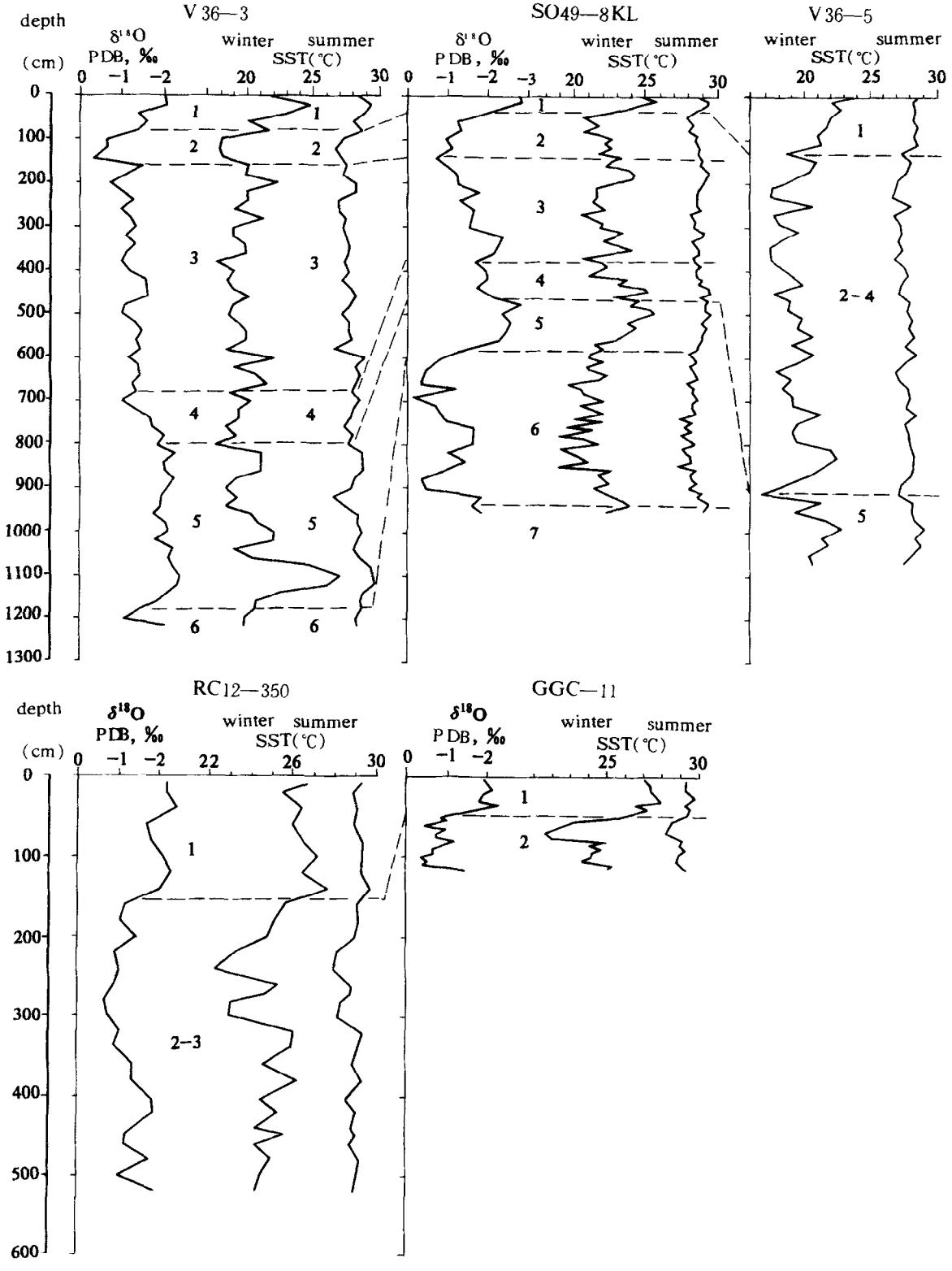
V 36—3
SO49—8KL
V 36—5
RC12—350
GGC—11
depth
(cm)
δ18O
PDB, ‰
winter
summer
SST(℃)

(Fig. 5C and D). The winter SST ranges from 17.5°C in the north to 23°C in the south, displaying a N–S trend, whereas the pattern of summer SST shows a E–W trend, increasing from less than 25°C in the east to 27°–28°C in the west. The glacial SST patterns are very different than the modern ones (Fig. 5A and B). As the SST patterns depend on the surface circulation, the differences must be caused by circulation changes.

3.4. Surface circulation

The sea surface circulation in the modern SCS is driven basically by the East Asian Monsoon. With the seasonal alternation of prevailing wind, i.e. the southwest monsoon in summer and northeast monsoon in winter, the SCS displays a transbasinal pattern of surface currents with opposite directions during summer and winter (Fig. 6A and

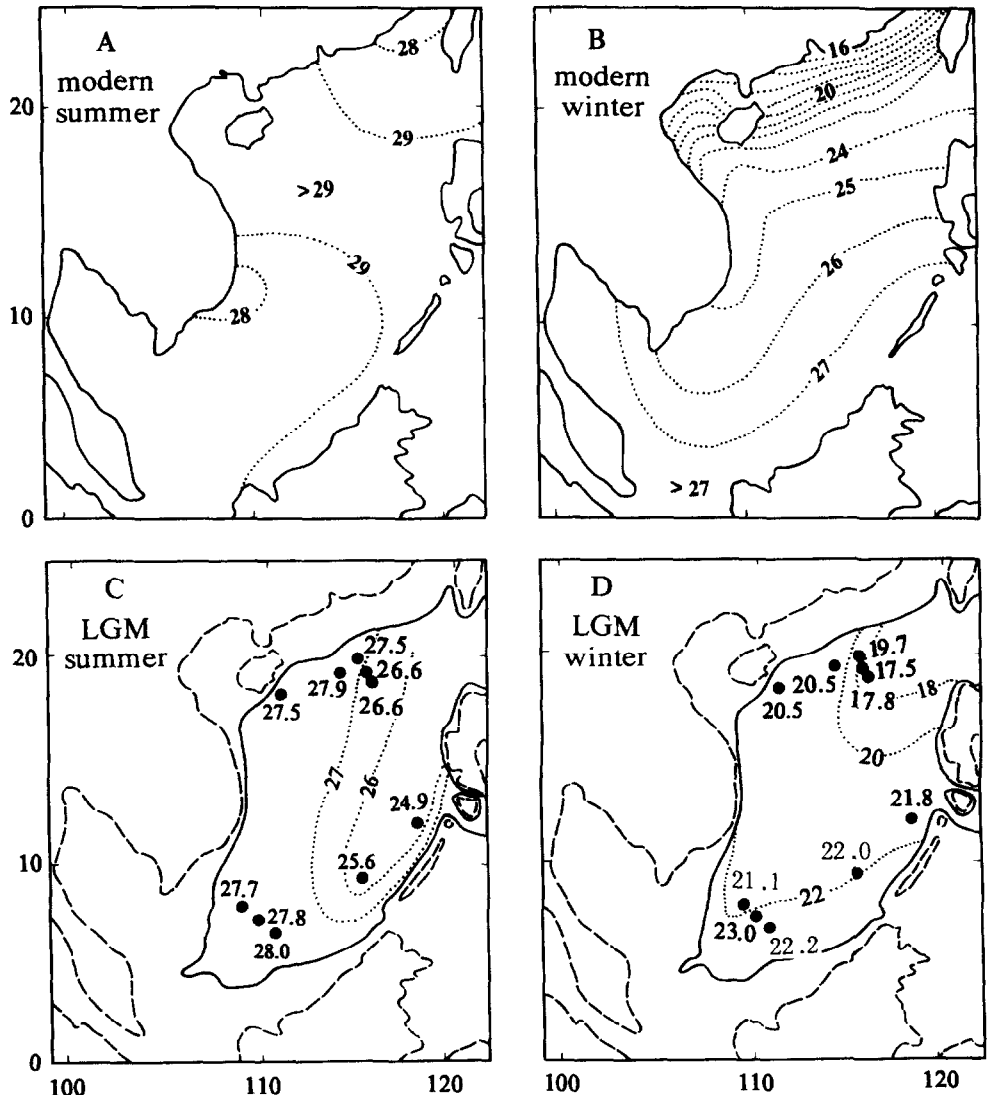

Fig. 5. Average sea surface temperature in the South China Sea (°C). (A) Modern, summer; (B) modern winter; (C) last glacial maximum, summer; (D) last glacial maximum, winter. Dotted lines denote isotherms (°C). (A and B) from Wang and Wang (1990).

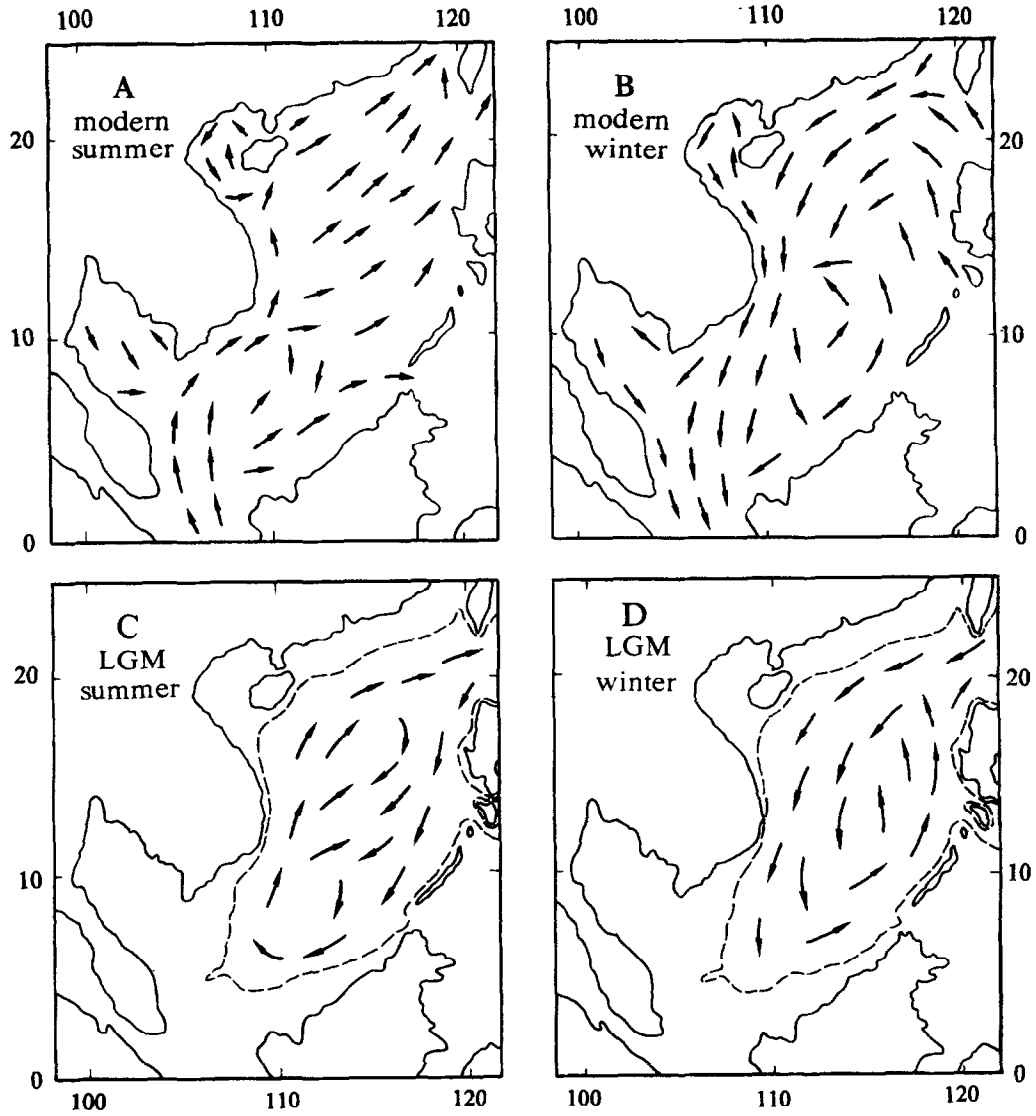

Fig. 6. Surface circulation patterns of the South China Sea. (A) Modern, summer; (B) modern, winter; (C) last glacial maximum, summer; (D) last glacial maximum, winter (see text).

B). In summer, surface water of the tropical Indian Ocean flows into the SCS northward and then into the Pacific, mostly through Bashi Strait. The inflow of warm tropical water from the Indian Ocean has given rise to insignificant variations of modern summer SST in plan (28°–29°C; Fig. 5A). In winter the northeast wind drives the tropical and subtropical Pacific waters together with the cooler water of longshore current into the SCS through Bashi and Taiwan Straits and then across the Sunda shelf into the Indian Ocean. The inflow of the cooler water from the north has led to a steeper temperature gradient in the winter SCS: from 16°C in the northern inner shelf to 27°C in the south (Fig. 5B).

Meanwhile, the surface circulation is also constrained by the configuration of the sea. Topographically, the southern part of the SCS is a shallow shelf and must have been emerged during the last glacial maximum (LGM) when the global

sea level decreased by some 120 m. On the northern side the SCS has two connecting channels: the Taiwan Strait and the Bashi Strait with sill depths of around 70 m and 2500 m, respectively; on its eastern side there are Mindora Strait (open to the Sulu Sea) and Balabac Strait with sill depth of 450 and 100 m. During the LGM, when the sea level dropped by 100–120 m, all the southern connections to the ocean closed, and the SCS changed into a semi-enclosed basin with Bashi Strait as its only water passway to the ocean. A numerical simulation would show the changes in surface circulation brought on by the altered configuration.

Modern surface circulation of the SCS has been simulated by Chinese meteorologists with a numerical model based on 2D shallow-water equations, taking wind stress, bottom topography and coastal configuration into account (Zeng et al., 1989). As shown by a preliminary computer simulation with the changed coastal configuration corresponding to the low sea level at the LGM, the surface circulation patterns in the SCS should be radically different from the modern ones: the glacial surface circulation should be counter-clockwise for winter and basically clockwise for summer (Li, Rongfeng, pers. commun., 1992). Interglacial (and post-glacial) trans-basinal patterns of circulation must be replaced by semi-enclosed patterns as schematically shown in Fig. 6C and D.

On the other hand, the glacial circulation patterns in the Pacific should bring cooler water into the SCS. During LGM, polar front in the Western Pacific was shifted about 10° of latitudes to the south (Thompson, 1981) and, hence, temperate waters could reach the Bashi Strait, the only connection of the SCS with the Pacific during glacial episodes (Fig. 7). The inflow of cooler temperate waters into the northern SCS together with the cut-off of warm Indian Ocean waters on its south would have caused a considerable

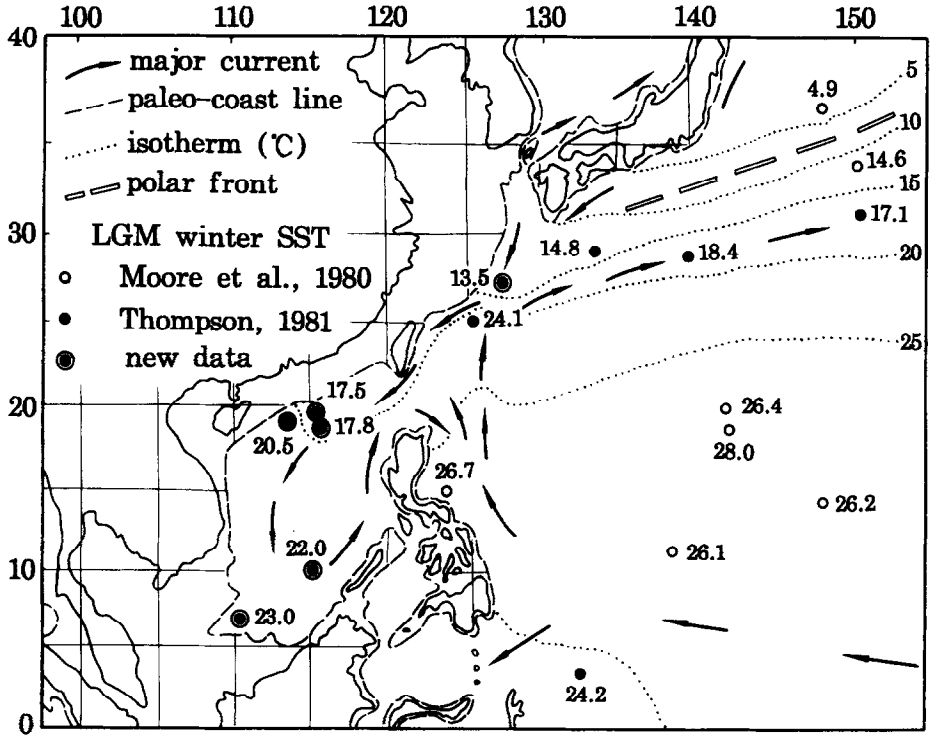

Fig. 7. Average winter sea surface temperature (°C) and major surface currents in the South China Sea and the adjacent Western Pacific at the last glacial maximum. Paleotemperature data from Moore et al. (1980), Thompson (1981), Wang and Wang (1990) and Li et al. (1992).

decrease of SST in the glacial SCS and an enhanced G/IG contrast in SST there, as recorded in sediment cores discussed above.

Moreover, the inflow of cooler waters into the SCS through its northeastern connection (Bashi Strait) must have affected the SST patterns during glacials. Since the inflowing water should be running southward in summer (clockwise circulation) and westward in winter (counter-clockwise circulation), the SST would be expected to be cooler in its eastern part for summer and in its northern part for winter. Our paleo-SST reconstructions show that it is the case (Fig. 5), and the different patterns of surface currents explain the E–W SST gradient for summer (Fig. 5C) and S–N gradient for winter (Fig. 5D).

3.5. *Younger Dryas event?*

The last deglaciation is of particular interest for the Past Global Change studies, and the high deposition rates make the SCS most promising in this respect. Therefore, the uppermost part of Core V36-3 (Table 1; Fig. 1) was restudied for a detailed history of the last deglaciation. The upper 1.6 m of the core section (representing approximately the last 25 kyr) was sampled with 4–5 cm intervals and analyzed for both stable isotopes and transfer function paleo-SST of planktonic foraminifers. The results of our analyses are partly provided in the present paper (Fig. 8).

From the SST curves in Fig. 7 an abrupt cooling event is seen at 0.74 m with a SST decrease of 2.7°C for winter and 0.9°C for summer, followed by a rapid temperature rise to the original level at 0.56 m. According to oxygen-isotope stratigraphy of the core, event 1.1 occurs at 0.25 m and 2.2 at 1.29 m. If the sedimentation rate between the two events is presumed to be stable and the chronostratigraphy by Martinson et al. (1987) is adopted, the cooling event should have occurred about at 10 ka, close to the Younger Dryas event

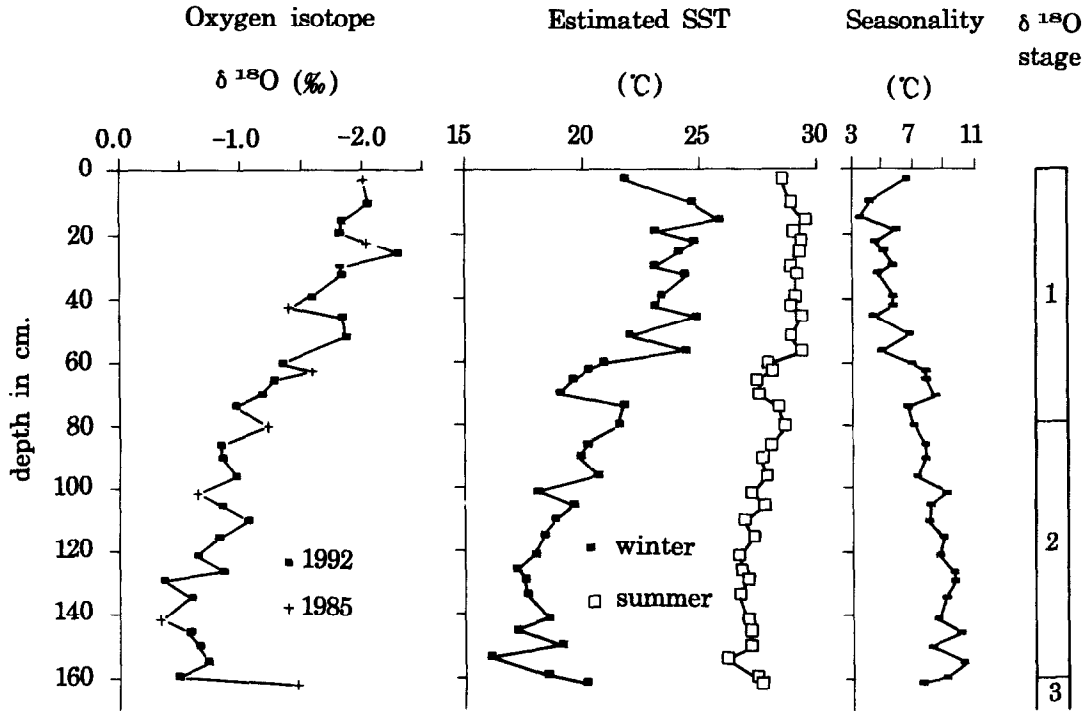

Fig. 8. Paleotemperature variations recorded in upper part of Core V36-3. Notice the Younger Dryas-style cooling event at 74 cm. Oxygen isotope curve of *Globigerinoides sacculifer* is based on two sets of measurements (1985 and 1992) made at the Godwin Laboratory, Cambridge; SST estimates are resulted from calculations using Transfer Function FP-12E; seasonality is the difference between estimated summer and winter SST (from Wang et al., 1994).

(Wang et al., 1994). As we are still waiting for AMS ^{14}C dating, no conclusion can be made yet for age of this event in Core V36-3. It is clear, however, that the core has recorded a Younger Dryas-style event and the glacial–postglacial transition in the SCS must not be straightforward (Wang et al., 1992a).

There is no unanimity in literature concerning the occurrence of the Younger Dryas outside the northern Atlantic region in general, and in the low latitude Pacific in particular. Based on AMS ^{14}C datings and weights of two foraminiferal species, Broecker et al. (1988b) reported an abrupt change in abundance of planktonic foraminifers and in sedimentation rate at the close of the last glaciation in Core V35-5, southern SCS, and denied the occurrence of the Younger Dryas in the region. However, the oxygen isotope and foraminiferal analyses have provided evidence for the Younger Dryas event in the adjacent Sulu Sea (Linsley and Thunell, 1990; Kudrass et al., 1991), and the Younger Dryas-like cooling event was found in oxygen-isotope curves from the SCS (Kudrass et al., 1992). Precise datings are badly needed to determine if the event(s) recorded in the SCS is the Younger Dryas.

4. Carbonate cycles

4.1. Previous work

The discovery of Pleistocene carbonate cycles in the equatorial Pacific early in the 1950s (Arrhenius, 1952) stands at the beginning of the revolution of our understanding of the Ice Ages and the climate cyclicity (Berger, 1992). Although it is still debated whether productivity or dissolution is responsible for the cycles (Berger, 1973, 1992; Arrhenius, 1988), there is no doubt that deep-sea carbonate cycles are of great significance in stratigraphic correlation, as well as for studies on carbon cycle and climate variations. Being a marginal sea of the West Pacific with widely distributed carbonate sediments, the SCS in expected to throw light on the matter.

Judging from the carbonate content and the preservation of planktonic foraminifers in surface sediments of the SCS, the modern CCD there has been found at 3500–3800 m, lysocline at about 3000 m and ACD (aragonite compensation depth) between 1000–1400 m (Rottman, 1979; Chen and Chen, 1983; Li, 1989; Thunell et al., 1992). Downcore fluctuations of $CaCO_3$% in Core V36-3, northern slope of the SCS, display a glacial decrease and interglacial increase of carbonate, resembling the carbonate curves reported from the North Atlantic, and this has been ascribed to the dilution by terrigenous clasts (P. Wang et al., 1986). A similar carbonate curves have been reported also from the southern part of the SCS (Core SCS-15A; C. Wang et al., 1986), from other cores in the northern SCS (Feng et al., 1988) and from the Okinawa Trough (Wang, 1990).

Our recent studies on pteropods (L. Wang, 1992) and foraminifers (Bian et al., 1992) have provided new evidence for aragonite and calcite dissolution in the SCS, enabling a relatively all-round view of the carbonate cycles there.

4.1. Material and methods

As mentioned above, the continental slope of the SCS above CCD is blanketed by calcareous silty clay or clayey silt where $CaCO_3$% ranges basically from 10 to 50%, but may exceed 60% near coral reefs (Table 1). The cores from the continental slope are most sensitive to carbonate cycles and, hence, are used as a basis for our following discussion.

Along with carbonate content ($CaCO_3$%) in bulk samples, abundance and preservation of pteropod (aragonite) and planktonic foraminiferal (calcite) shells in sediments, ratio between benthic and planktonic foraminifers ("benthic ratio"), ratio between fragments and entire tests of planktonic foraminifers ("fragments ratio"), and Foraminiferal Dissolution Index (FDX; Berger, 1979) are also used in this study. The downcore variations of foraminiferal abundance correspond well to those of the carbonate content and, thus, can be used to approximate the carbonate cycles when $CaCO_3$% data are absent. The FDX, benthic ratio and fragments ratio are indicative of carbonate dissolution and display a trend basically oppo-

site to the carbonate curve. Aragonite dissolution is estimated by pteropod abundance. All these values can be used to extract dissolution signals from the carbonate cycles.

4.2. Cycles above the modern lysocline

While comparing the $CaCO_3$% curves from the high latitude North Atlantic and the equatorial Pacific, Luz and Shackleton(1975) noticed two different trends nearly counter to each other: in the Atlantic the carbonate content in sediments increases in the glacial and decreases in the interglacial with the $CaCO_3$% curve running roughly parallel to the oxygen-isotope curve, whereas the Pacific curve displays a different trend with the minimal values at stages 4 and 5 (Fig. 9). In searching an explanation for the difference, Seibold and Berger (1982) attributed the Atlantic cycles to *dilution cycles* and those of the Pacific to *dissolution cycles*. The later studies, however, have shown more complicated variations in carbonate cycles of the two oceans, as the cause of these variations must be deeply rooted in changes of deep-water circulation and chemical reorganization in the world ocean (e.g., Crowley, 1985; Zahn et al., 1991).

In the SCS, the carbonate curves from sites above the present lysocline are basically concordant with the oxygen-isotope curves, showing glacial decrease and interglacial increase of carbonate proportion in sediment (Fig. 9). This can be illustrated with four cores raised from various water depths: V36-6 (water depth 1579 m; Fig. 10A), SCS-15A (1812 m; Fig. 10B), GGC-11 (2165 m; Fig. 10C) and V36-3 (2809 m; Figs. 9 and 11). There is no isotope data for Core V36-6, but the similarity of its carbonate curve with that of Core V36-3 has provided stratigraphic correlation. All the curves resemble those in high latitude north Atlantic and considerably differ from those in equatorial Pacific.

In order to explain the "Atlantic cycles" in the SCS, stage-by-stage variations in depositional rates of carbonate and non-carbonate components in Core V36-3 are calculated (Table 2). It turns out that the deposition rate of non-carbonate material (mainly clay in this case) decreases from 9.5 cm/kyr for the glacial (stages 2–4) to 5–6 cm/kyr for the inter- and post-glacial (stages 1 and 5), implying a significantly intensified input of terrigenous material into the sea basin during glacial what is the main mechanism behind the "Atlantic type" of carbonate cycles in the SCS. As to the deposition rate of $CaCO_3$, no glacial–interglacial contrast is observed. It remains almost stable in the upper part of the core (close to 1.5 cm/kyr), but decreases to 1.2 cm/kyr in stage 5 obviously due to dissolution (see below). Thus, the carbonate cycles in the SCS above lysocline are caused by the terrigenous input and belong to dilution cycles (P. Wang et al., 1986).

4.3. Cycles below the modern lysocline

Despite of their wide distribution in the SCS, the "Atlantic cycles" are limited to water depths above the modern lysocline. Below 3500 m, carbonate curves belong to a different type as exemplified by Core SO50-29KL from the northern slope (water depth 3766 m; Fig. 12A and B). With carbonate content mostly less than 10%, the $CaCO_3$ curve of the core runs almost counter to the oxygen isotope curve, and the minimal values occur in stages 4 and 5, a feature common to the equatorial Pacific.

Noticeable is the similarity between $CaCO_3$ curve in Core SO50-29KL and that of planktonic foraminiferal abundance in Core SO49-14KL (water depth 3624 m; Fig. 12C), again below the modern lysocline. Both curves show peaks at the early part of stage 3 and late part of stage 2, and the lowest values occur at stages 4, 5 and late part of stage 3. The same trend is seen in the carbonate curve of Core GGC-1 (water depth 4203 m; Fig. 12D), although at that site only stages 1–3 have been recovered. Again, the carbonate curve peaks at glacial, late in stage 2, and declines toward both stages 1 and 3. Cores GGC-2 (water depth 4010 m), GGC-3 (3725 m) and GGC-4 (3530 m), also from the eastern SCS below CCD, show the same picture (Thunell et al., 1992).

Summarizing carbonate records of stages 1–3 in all the transect of 12 cores (GGC-1 to GGC-13) in the eastern SCS off the Philippines, Thunell et al. (1992) pointed out that cores below CCD

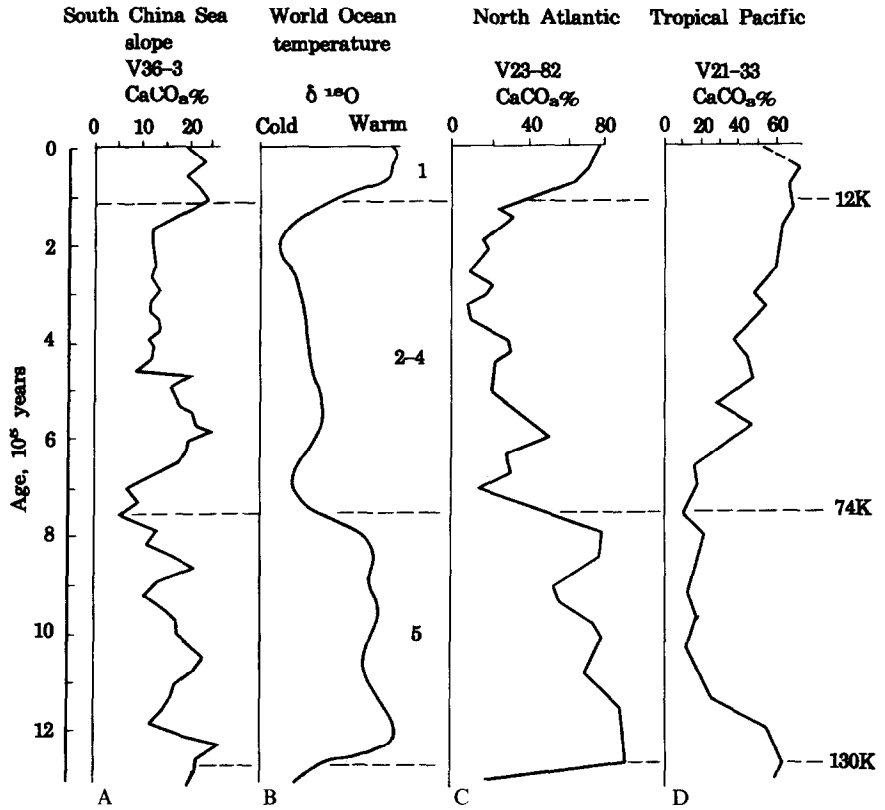

Fig. 9. Comparison of the late Quaternary carbonate curves of Core V36-3, northern South China Sea (A), with those in the high latitude North Atlantic (B, typified by Core V23-82) and the Equatorial Pacific (C, typified by Core V21-33). Notice the similarity between the curves (A) and (C) with the oxygen isotope curve (B). (From P. Wang et al., 1986; C and D after Luz and Shackleton, 1975.)

(3800 m) display "the typical Pacific carbonate pattern (high carbonate during glacials and low carbonate during interglacials)". In general, our synthesized data from stages 1–5 throughout the SCS show the same trend, but more complicated than the above generalization.

4.4. Dilution and dissolution cycles

In Core SO49-14KL, the curve of planktonic foraminiferal abundance swings counter to that of "benthic ratio", suggesting a dissolution control of carbonate cycles there. The dissolution index FDX shows its peaks at stages 1, 3, and 5, implying strengthened dissolution during interglacials. The same is true for other cores below lysocline (Bian et al., 1992). Thus, there are two types of carbonate cycles in the SCS: dilution-controlled cycles above lysocline and dissolution-controlled cycles below lysocline.

However, dissolution may occur at sites above lysocline as well. In Core V36-6, for example, $CaCO_3$ curve displays a opposite trend to that of FDX (Fig. 10A). The curve of "benthic ratio" and that of FDX, in general, run parallel to each other, but nearly opposite to the $CaCO_3$ curve (Fig. 11). All these have demonstrated the dissolution effect of foraminiferal calcite tests even above lysocline.

Based on pteropod distribution in surface sediments, Rottman (1979) has found the ACD in the SCS being about 1000 m. The site of Core SO49-8KL (water depth 1040 m) lies just below the present ACD and is most sensitive to its

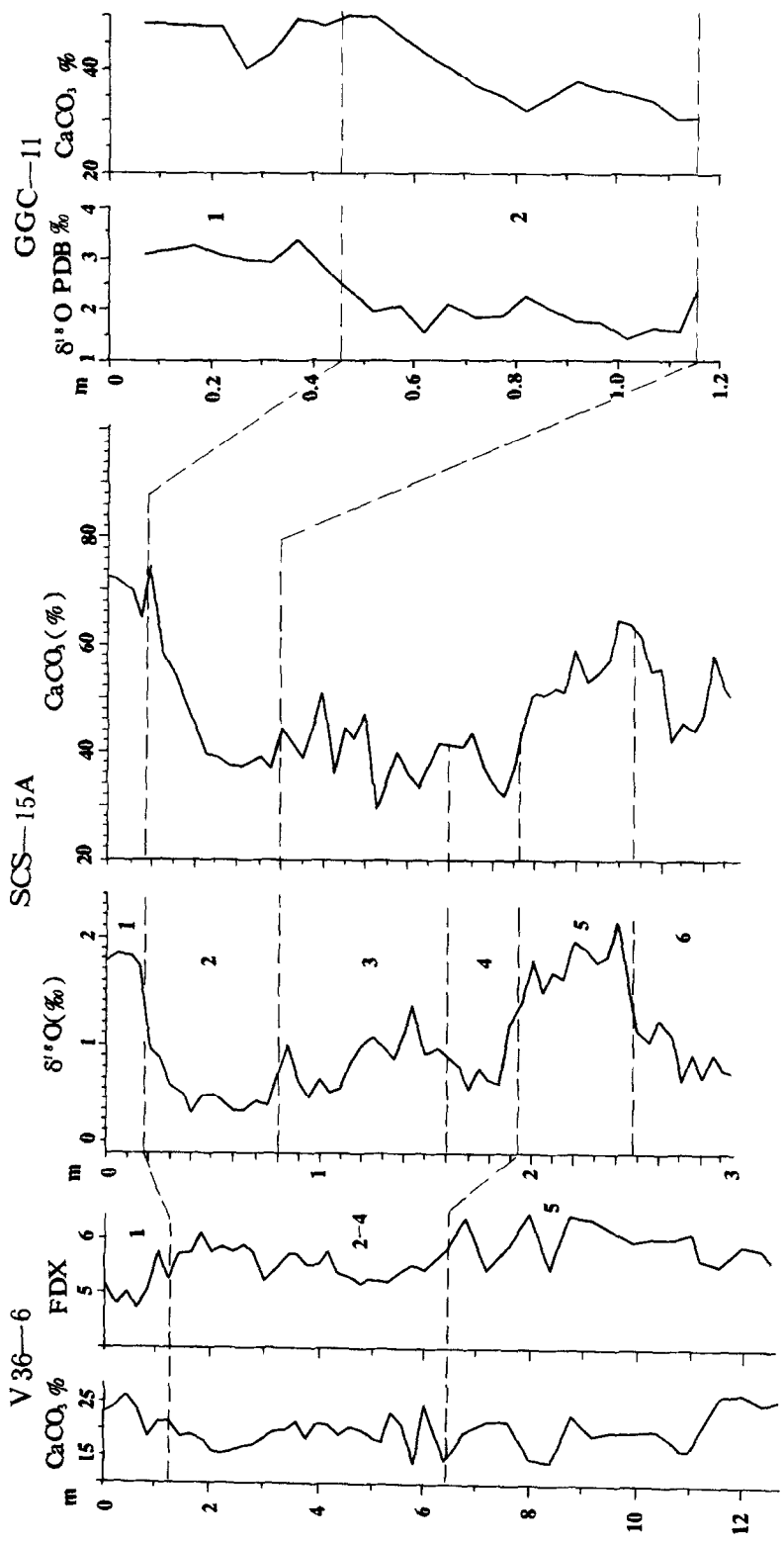

Fig. 10. Carbonate curves of 3 cores in the South China Sea above the modern lysocline. (A) V36-6 (water depth 1579 m; from Bian et al., 1992); (B) SCS-15A (1812 m; from C. Wang et al., 1986); (C) GGC-11 (2165 m; after Thunell et al., 1992). Oxygen isotopes are measurements on *Globigerinoides sacculifer*. FDX denotes Foraminiferal Dissolution Index using 7-grade classification (Berger, 1979). Stratigraphy of V36-6 is based on correlation of its $CaCO_3$ curve with that of V36-3 provided with oxygen-isotope data. For location see Fig. 1 and Table 1.

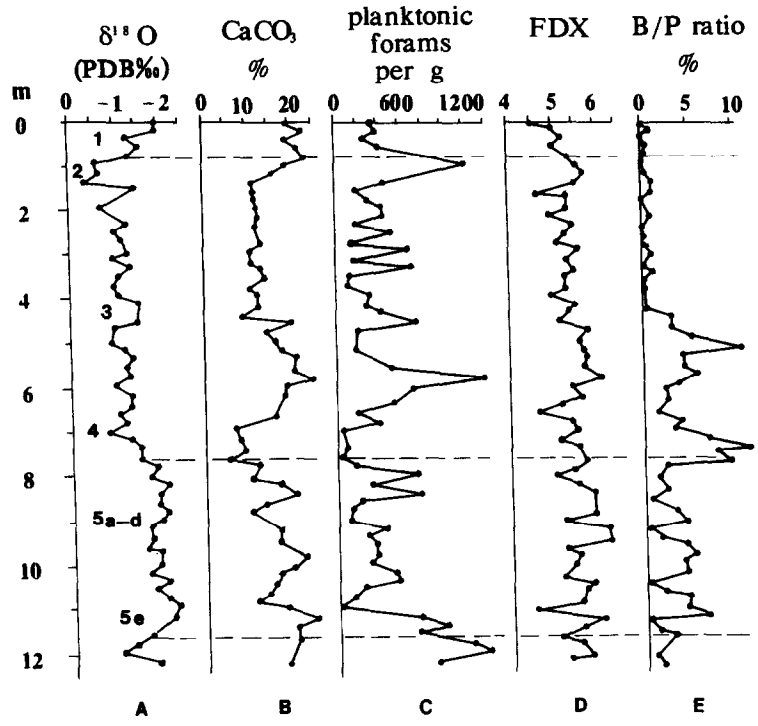

Fig. 11. Downcore variations of foraminiferal indications of carbonate dissolution compared with $CaCO_3$ and oxygen isotope curves in Core V36-3. FDX denotes Foraminiferal Dissolution Index using 7-grade classification (Berger, 1979). B/P denotes ratio between the abundance of planktonic and benthic foraminifera ("benthic ratio").

Table 2
Late Quaternary deposition rates for various stages in Core V36-3 (modified from P. Wang et al., 1986)

$\delta^{18}O$ stage	Depth (cm)	No. of samples	Duration (year)	Thickness of sediments (cm)	Deposition rate (km/yr)	$CaCO_3$% (average)	Deposition rate (cm/kyr)		FDX
							$CaCO_3$	non-$CaCO_3$	
1	0–82	5	12,000	82	6.83	21.18	1.46	5.37	5.1
2–4	82–762	34	62,000	680	10.97	13.49	1.48	9.49	5.4
5	762–1162	20	56,000	400	7.14	17.00	1.21	5.93	5.6

fluctuations. As shown by the recent analysis of the core, pteropods occur only in glacial sections of stages 2 and 6 where abundance of planktonic foraminifers also reaches its peaks (L. Wang, 1992). An almost opposite trend is shown in curves of "benthic ratio" and "fragments ratio", both indicative of calcite dissolution (Fig. 13). It is suggested, therefore, the ACD falls down during the glacial when the effect of calcite dissolution is decreased as well.

To sum up, the late Quaternary carbonate cycles in the SCS are resulted from superimposition of dissolution and dilution cycles. During the glacial low stands of sea level, increased input of terrigenous clasts raises sedimentation rate and dilutes carbonate, producing "Atlantic cycles". Since the

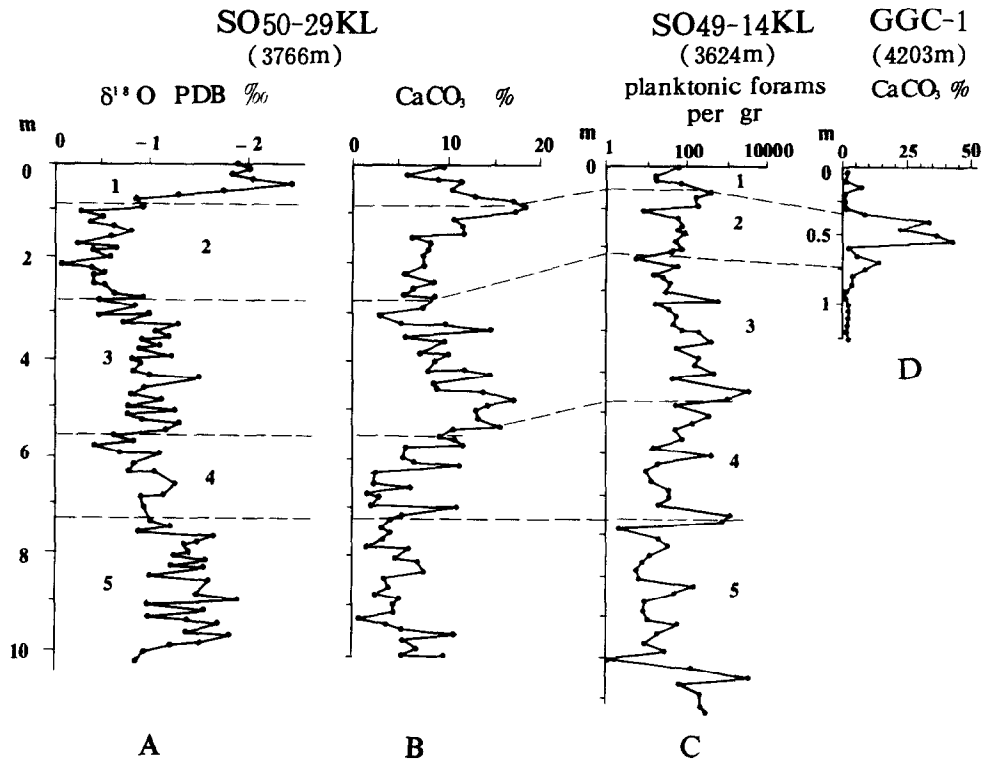

Fig. 12. Carbonate curves of 3 cores in the South China Sea below the modern lysocline. (A and B) SO50-29KL (from Zheng and Chen, in press); (C) SO49-14KL showing abundance of planktonic foraminifers (from Bain et al., 1992); (D) GGC-1 (from Thunell et al., 1992). For location see Fig. 1 and Table 1.

terrigenous material is mainly provided by river, the effect is most significant near estuaries at not too deep sites. On the other hand, the continuous connection between the SCS and the Pacific leads to a similarity in their water chemistry. All the studied cores taken from the SCS share the same carbonate dissolution signals as the Pacific. Regardless of depth position below or above the modern lysocline, dissolution of both calcite and aragonite is strengthened during stages 5 and 4 in the SCS, a common feature recorded in the western equatorial Pacific (e.g., Core EEDC-93P, water depth 1619 m; Core RC17-177, 2600 m; core V28-328, 3120 m; see Le and Shackleton, 1992) attributed to an uplifted lysocline (Farell and Prell, 1989). The role of the two factors depends on water chemistry: Above the modern lysocline dilution effect predominates and the "Atlantic cycles" are produced, below the lysocline dissolution effect prevails and the "Pacific" pattern is recorded.

5. Conclusions

(1) In the SCS the Holocene deposition rate of hemipelagic sediments can be as high as 15 cm/kyr because of the considerable terrigenous supply by the rivers. The maximum values occur in two areas off the Pearl River and paleo-North Sunda River mouths where the deposition rate may reach 31 cm/kyr in the last glacial.

(2) There are two types of late Quaternary carbonate cycles in the deep-water sediments of the SCS. As a basin with a large humid catchment area, the terrigenous supply to the SCS raises during glacial stages what increases deposition

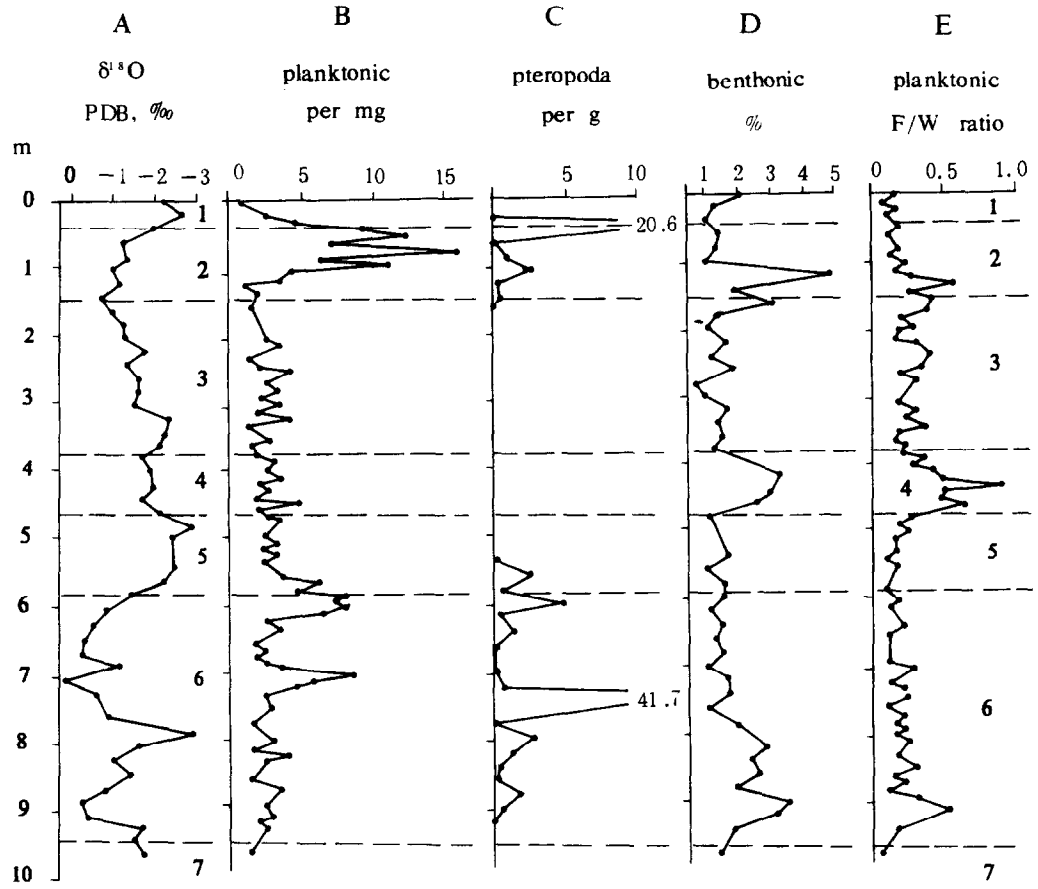

Fig. 13. Downcore variations of foraminiferal and pteropod abundance as carbonate dissolution indications in Core SO49-8KL. (A) Oxygen isotope of *Globigerinoides sacculifer*; (B) abundance of planktonic foraminifers per milligram sediment; (C) abundance of pteropods per gram sediment; (D) percentage of benthic foraminifers in total fauna; (E) ratio of fragments to whole tests of planktonic foraminifers (from Bian et al., 1992). For location see Fig. 1 and Table 1.

rates on one hand and dilutes carbonate content in sediment on the other, leading to the "Atlantic cycles" above the modern lysocline. Below the lysocline, deep-sea carbonate dissolution prevails over the dilution effect; since the late Quaternary carbonate cycles there display the "Pacific" pattern, it implies a continuous water exchange and chemical concordance, at least for carbonate saturation, of the SCS with the West Pacific.

(3) During glacial intervals, the cut-off of the tropical Indian Ocean waters on the south and the inflow of the temperate Pacific water on the north have caused enhanced G/IG contrasts in SST in the SCS (6.8°–9.3°C in the northern slope). Due to the alterations in its coastal configuration, the transbasinal patterns of interglacial surface circulation is replaced by the glacial semi-enclosed patterns. The counterclockwise circulation in glacial winter gives rise to a S–N gradient in SST, and the clockwise circulation in glacial summer leads to a E–W gradient in SST, as recorded in analyzed sediment cores.

(4) In the SCS an Younger Dryas-style abrupt cooling event occurred in the last deglaciation and recorded in high-resolution sequences of transfer function paleotemperatures and oxygen isotopes. AMS ^{14}C datings are needed to identify if the event is equal to the Younger Dryas in the North Atlantic.

(5) Among the marginal seas in the West Pacific,

the SCS has been proved to be one of the basins most informative and sensitive to environmental changes in glacial cycles. Thanks to its sill depth of about 2500 m, the SCS is favourable for monitoring the glacial changes of deeper waters in the Northern Pacific, and this is the problem where the further studies should be focused.

Acknowledgements

We gratefully acknowledge the Lamont–Doherty Geological Observatory Deep-Sea Sample Repository (supported by NSF through Grant OE88-0001 and Office of Naval Research through Grant N00014-87-K0204), the Institute of Oceanography, Taiwan University, the Second Institute of Oceanography, SOA of China, Second Marine Geological Investigation Brigade, MGMR of China, for supplying core samples. Financial support for the study came from the Chinese National Science Foundation and the National Commission for Education of China. M. Hall and J. Le, Cambridge, are thanked for the stable isotope analyses, and M. Wu and Mr. Z. Liu, Shanghai, for their technical assistance in preparing the manuscript.

References

Andree, M., Oeschger, H., Broecker, W.S., Beavan, N., Mix, A., Bonani, G., Hofmann, H.J, Morenzoni, E., Nessi, M., Suter, M. and Wolfli, W., 1986. AMS radiocarbon dates on foraminifera from deep sea sediments. Radiocarbon, 28(2A): 424–428.

Arrhenius, G.O.S., 1952. Sediment Cores from the east Pacific. Rep. Swed. Deep Sea Exped. 1947–1948, 5, 288 pp.

Arrhenius, G.O.S., 1988. Rate of production, dissolution and accumulation of biogenic solids in the ocean. Palaeogeogr., Palaeoclimatol., Palaeoecol., 67: 119–146.

Berger, W.H., 1973. Deep-sea carbonates: Pleistocene dissolution cycles. J. Foraminiferal Res., 3: 187–195.

Berger, W.H., 1979. Preservation of Foraminifera. In: Foraminiferal Ecology and Paleoecology. SEPM Short Course, 6: 105–155.

Berger, W.H., 1987. Ocean ventilation during the last 12,000 years: hypothesis of counterpoint deep water production. Mar. Geol., 78: 1–10.

Berger, W.H., 1992. Pacific carbonate cycles revisited: arguments for and against productivity control. In: K. Ishizaki and T. Saito (Editors), Centenary of Japanese Micropaleontology. Terra Publ., Tokyo, pp. 15–25.

Bian, Yunhua, Wang, Pinxian and Zheng, Lianfu, 1992. Deep-water dissolution cycles of late Quaternary planktonic foraminifera in the South China Sea. In: Z. Ye and P. Wang (Editors), Contributions to Late Quaternary Paleoceanography of the South China Sea. Qingdao Ocean Univ. Press, Qingdao, pp. 261–273 (in Chinese, with English abstr.).

Broecker, W.S., Andree, M., Bonani, G., Wolfli, W., Klas, M., Mix, A. and Oeschger, H., 1988a. Comparison between radiocarbon ages obtained on coexisting planktonic foraminifers. Paleoceanography, 3(6): 647–657.

Broecker, W.S., Andree, M., Klas, M., Bonani, G., Wolfli, W. and Oeschger, H., 1988b. New evidence from the South China Sea for an abrupt termination of the last glacial period. Nature, 333: 156–158.

Chen, Muhong and Chen, Shaomou, 1989. On the carbonate dissolution and the distribution model of deep sea sediment types in the South China Sea. Tropical Oceanography, 8(3): 20–26 (in Chinese, with English abstr.).

Crowley, T.J., 1985. Late Quaternary carbonate changes in the North Atlantic and Atlantic/Pacific comparisons. In: E. Sundquist and W. Broecker (Editors), The Carbon Cycle and Atmospheric CO_2: Natural Variations Archean to Present. Am. Geophys. Union, pp. 271–284.

Duplessy, J.C., Bard, E., Arnold, M., Shackleton, N.J., Duprat, J. and Labeyrie, L., 1991. How fast did the ocean–atmosphere system run during the last deglaciation? Earth Planet. Sci. Lett., 103: 27–40.

Farrell, J.W. and Prell, W.L., 1989. Climate change and $CaCO_3$ preservation: an 800,000 year bathymetric reconstruction from the central equatorial Pacific Ocean. Paleoceanography, 4: 447–466.

Feng, Wenke, Xue, Wanjun and Yang, Dayuan, 1988. The Geological Environment of Late Quaternary in the Northern South China Sea. Guangdong Sci. Technol. Publ. House, Guangzhou, 261 pp. (in Chinese, with English abstr.).

Gao, Liang, Yan, Jun and Xue, Shengji, 1992. Late Quaternary paleoceanography in the northwest shelf of the South China Sea. In: Z. Ye and P. Wang (Editors), Contributions to Late Quaternary Paleoceanography of the South China Sea. Qingdao Ocean Univ. Press, Qingdao, pp. 96–107 (in Chinese, with English abstr.).

Gu, Zhaoyan, Liu, Tungsheng, Chen, Mingyang, Zheng Shuhui, Chen, Chengye and Liu, Yan, 1991. The oxygen isotopic composition of the foraminifera in the sediments from the South China Sea. Quaternary Sciences, 1991(1): 55–63 (in Chinese, with English abstr.).

Hao, Yichun et al., 1989. Quaternary Microbiotas and their Geological Significance from Northern Xisha Trench of South China Sea. China Univ. Geosci. Press, Wuhan, 223 pp. (in Chinese, with English abstract).

Jian, Zhimin, 1992. Sea surface tempeatures in the southern continental slope of the South China Sea since last glacial and their comparison with those in the northern slope. In: Z. Ye and P. Wang (Editors), Contributions to Late

Quaternary Paleoceanography of the South China Sea. Qingdao Ocean Univ. Press, Qingdao, pp. 78–87 (in Chinese, with English abstr.).

Kudrass, H.R., Erlenkeuser, H., Vollbrecht, R. and Weiss, W., 1991. Global nature of the Younger Dryas cooling event inferred from oxygen isotope data from Sulu Sea cores. Nature, 349: 406–408.

Kudrass, H.R., Schonfeld, J., Erlenkeuser, H., Winn, K. and Von Grafenstein, R., 1992. The last glacial–interglacial transition in the South China Sea recorded by stable isotope of benthic and planktonic foraminifera (Abstr.). 4th Int. Conf. Paleoceanogr. (21–25 September 1992, Kiel.) Progr. Abstr., p. 170.

Le, J. and Shackleton, N.J., 1992. Carbonate dissolution fluctuations in the western equatorial Pacific during the late Quaternary. Paleoceanography, 7(1): 21–42.

Li, Cuizhong, 1989. Deep water carbonate sedimentation of the South China Sea. Acta Sedimentol. Sinica, 7(2): 35–44 (in Chinese, with English abstr.).

Li, Cuizhong, 1993. Micropaleontology, carbonates and oxygen isotope records in late Quaternary deep-water sediment cores of the South China Sea. Trop. Oceanogr. 12(1): 16–23 (in Chinese, with English abstr.).

Li, Liangquan, Tu, Xia, Luo, Youlang and Chen, Shaomou, 1992. Planktonic foraminiferal assemblages and paleoceanography of South China Sea in late Quaternary. Trop. Oceanogr., 11(2): 62–69 (in Chinese, with English abstr.).

Linsley, B.K. and Thunell, R.C., 1990. The record of deglaciation in the Sulu Sea: evidence for the Younger Dryas event in the tropical Western Pacific. Paleoceanography, 5(6): 1025–1039.

Luz, B. and Shackleton, N.J., 1975. $CaCO_3$ solution in the tropical East Pacific during the past 130,000 years. In: A.W.H. Bé and W.H. Berger (Edotors), Dissolution of Deep-sea Carbonates. Spec. Publ. Cushman Found. Foraminiferal Res., 13: 142–150.

Martinson, D.G., Pisias, N.G., Hays, J.D., Imbrie, J., Moore, T.C., Jr. and Shackleton, N.J., 1987. Age dating and the orbital theory of the Ice Ages: development of a high-resolution 0 to 300,000-year chronostratigraphy. Quat. Res., 27: 1–29.

Min, Qiubao, Zhao, Quanhong, Wang, Pinxian and Feng, Wenke, 1992. Paleoceanography of the outer shelf, northern South China Sea: a preliminary study. In: Z. Ye and P. Wang (Editors), Contributions to Late Quaternary Paleoceanography of the South China Sea. Qingdao Ocean Univ. Press, Qingdao, pp. 108–118 (in Chinese, with English abstr.).

Moore, T.C., Jr., Burckle, L.H., Geitzenauer, K., Luz, B., Molina-Cruz, A., Robertson, J.H., Sache, H., Sancetta, C., Thiede, J., Thompson, P. and Wencam, C., 1980. The reconstruction of sea surface temperature in the Pacific Ocean of 18,000 B.P. Mar. Micropaleontol., 5: 215–247.

Rottman, M.L., 1979. Dissolution of planktonic foraminifera and pteropods in South China Sea sediments. J. Foraminiferal Res., 9(1): 41–49.

Samodai, J.P., Thompson, P. and Chen, Chin, 1986. Foraminiferal analysis of South China Sea core V36-08 with paleoenvironmental implications. Proc. Geol. Soc. China, Taipei, 29: 118–137.

Seibold, E. and Berger, W.H., 1982. The Sea Floor. An Introduction to Marine Geology. Springer, Berlin, 288 pp.

Thompson, P.R., 1981. Planktonic foraminifera in the western North Pacific during the past 150,000 years: comparison of modern and fossil assemblages. Palaeogeogr., Palaeoclimatol., Palaeoecol., 35: 241–279.

Thompson, P.R., Bé, A.W.H., Duplessy, J.C. and Shackleton, N.J., 1979. Disappearence of pink-pigmented *Globigerinoides ruber* at 120,000 yr B.P. in the Indian and Pacific Oceans. Nature, 280: 554–558.

Thunell, R.C., Miao, Qingmin, Calvert, S.E. and Pedersen, T.F., 1992. Glacial–Holocene biogenic sedimentation patterns in the South China Sea: productivity variations and surface water pCO_2. Paleoceanography, 7(2): 143–162.

Wang, Chung-Ho and Chen, Min-Pen, 1990. Upper Pleistocene oxygen and carbon isotopic changes of core SCS-15B at the South China Sea. J. SE Asian Earth Sci., 4(3): 243–246.

Wang, Chung-Ho, Chen, Min-Pen, Lo, Shen-Chung and Wu, Jong-Chang, 1986. Stable isotope records of late Pleistocene sediments from the South China Sea. Bull. Inst. Earth Sci., Acad. Sin., Taipei, 6: 185–195.

Wang, Luejiang, 1992. Late Quaternary pteropods and aragonite compensation depth in the northern South China Sea. In: Z. Ye and P. Wang (Editors), Contributions to Late Quaternary Paleoceanography of the South China Sea. Qingdao Ocean Univ. Press, Qingdao, pp. 249–260 (in Chinese, with English abstr.).

Wang, Luejiang and Wang, Pinxian, 1988. An attempt at paleotemperature estimation in South China Sea using transfer function. Chin. Sci. Bull., 34(11): 53–56.

Wang, Luejiang and Wang, Pinxian, 1990. Late Quaternary paleoceanography of the South China Sea: glacial–interglacial contrasts in an enclosed basin. Paleoceanography, 5(1): 77–90.

Wang, Luejiang, Bian, Yunhua and Wang, Pinxian, 1994. Last deglaciation and abrupt cooling events in the northern South China Sea. Quat. Sci., 1994(1): 1–12 (in Chinese, with English abstr.).

Wang, Pinxian, 1990. The Ice-Age China Sea—research results and problems. In: P. Wang, Q. Lao and Q. He (Editors), Proc. 1st Int. Conf. Asian Marine Geology. (7–10 September 1988, Shanghai.) China Ocean Press, Beijing, pp. 181–197.

Wang, Pinxian, in press. Paleoceanography in China: progress and problems. In: Y. Liang, D. Zhou and C. Zeng (Editors), Oceanology of China Seas. Kluwer, Dordrecht.

Wang, Pinxian and Sun, Xiangjun, 1995. Last glacial maximum in China: comparison between land and sea. Catena, 23: 341–353.

Wang, Pinxian, Wang, Luejiang and Bian, Yunhua, 1992a. The last deglaciation in the South China Sea (Abstract). 4th Int. Conf. Paleoceanography. (21–25 September 1992, Kiel.) Progr. Abstr., p. 294.

Wang, Pinxian, Jian, Zhimin and Liu, Zhiwei, 1992b. Late Quaternary sedimentation rate in the South China Sea. In: Z. Ye and P. Wang (Editors), Contributions to Late Quaternary Paleoceanography of the South China Sea. Qingdao Ocean Univ. Press, Qingdao, pp. 23–41 (in Chinese, with English abstr.).

Wang, Pinxian, Min, Qiubao, Bian, Yunhua and Feng, Wenke, 1986. Planktonic foraminifera in the continental slope of the northern South China Sea during the last 130,000 years and their paleoceanographic implications. Acta Geol. Sin. (Trial English Ed.), 60: 1–11.

Winn, K., Zheng, Lianfu, Erlenkeuser, H. and Stoffers, P., 1992. Oxygen/carbon isotopes and paleoproductivity in the South China Sea during the past 110,000 years. In: X. Jin, H.R. Kudrass and G. Pautot (Editors), Marine Geology and Geophysics of the South China Sea. China Ocean Press, Beijing, pp. 154–166.

Zahn, R., Rushdi, A., Pisias, N.G., Bornhold, B.D., Blaise, B. and Karlin, R., 1991. Carbonate deposition and benthic $\delta^{13}C$ in the subarctic Pacific: implications for changes of the oceanic carbonate system during the past 750,000 years. Earth Planet. Sci. Lett., 103: 116–132.

Zeng, Qingcun, Li, Rongfeng, Ji, Zhongzhen, Gan, Zijun and Ke, Peihui, 1989. Calculations of the monthly mean ocean currents of the South China Sea. Chin. J. Atmos. Sci., 13(2): 129–144.

Zheng, Lianfu and Chen, Wenbin (Editors), in press. Contributions to Sedimentation and Geochemistry of the South China Sea. China Ocean Press (in Chinese, with English abstr.).